NANO LETTERS

2008
Vol. 8, No. 4
988-996

Lotus Effect in Engineered Zirconia

Fereydoon Namavar,*,†,‡ Chin Li Cheung,*,‡,§ Renat F. Sabirianov,△ Wai-Ning Mei,△ Xiao Cheng Zeng,§ Gonghua Wang,§ Hani Haider,† and Kevin L. Garvin†

Department of Orthopaedic Surgery and Rehabilitation, 985360 Nebraska Medical Center, Omaha, Nebraska 68198-5360, Nebraska Centre for Materials and Nanoscience, University of Nebraska−Lincoln, Lincoln, Nebraska 68588, Department of Chemistry, University of Nebraska−Lincoln, 514A Hamilton Hall, Lincoln, Nebraska 68588, and Department of Physics, University of Nebraska, 6001 Dodge Street, Omaha, Nebraska 68182

Received August 25, 2007; Revised Manuscript Received January 24, 2008

ABSTRACT

Patterned micro- and nanostructured surfaces have received increasing attention because of their ability to tune the hydrophobicity and hydrophilicity of their surfaces. However, the mechanical properties of these studied surfaces are not sufficiently robust for load-bearing applications. Here we report transparent nanocrystalline ZrO_2 films possessing combined properties of hardness and complete wetting behavior, which are expected to benefit tribology, wear reduction, and biomedical applications where ultrahydrophilic surfaces are required. This ultrahydrophilic behavior may be explained by the Wenzel model.

In recent years, the lotus effect[1] and self-cleaning surfaces[2] have been investigated because of their scientific merit and potential practical applications. Fabrication of hydrophilic titanium oxide films has been reported; however, this property disappears after a short time.[3] In this letter, we report the growth of ultrahydrophilic and transparent nanocrystalline cubic and mixed phase zirconium oxide (ZrO_2) films produced by ion beam assisted deposition (IBAD).[4–7] This nanostructurally stabilized chemically pure cubic phase has been shown[8] to possess hardness as high as 16 GPa and a bulk modulus of 235 GPa,[8] which is in good agreement with a model calculation based on a projector augmented wave first-principles method.[9] Furthermore, first-principles calculations[9,10] indicated that both the modulus and surface energy of cubic ZrO_2 phase is larger than those for both monoclinic and tetragonal phases.

The scientific community[4] has been actively pursuing the study of IBAD for specific applications such as tribological coatings, anticorrosion coatings, optical coatings, superconducting buffer layers, and coatings for temperature sensitive substrates such as polymer. In this work, we have applied IBAD to produce ultrahydrophilic surfaces by producing well-defined nanostructures to increase the ratio[11] of true surface area to apparent surface area ($A_{true}/A_{apparent}$). IBAD (Figure 1) combines evaporation with concurrent ion beam bombardment in a high vacuum environment. Energetic ions (with a depth penetration of typically less than 20 nm) were employed to produce engineered nanocrystals "stitched" to a substrate *(utilizing billions and billions of directed and parallel ionic hammers)*. An ion beam can enhance film adhesion[12–15] in a number of ways by: (a) in situ removing of monolayers of contaminants prior to deposition, (b) increasing the reactivity of substrate/coating atoms, (c) generating a nanoscopically rough surface (interface), (d) increasing nucleation density, (e) increasing surface mobility (at a nanoscale) of coating atoms, and (f) decreasing formation of interfacial voids. Ion bombardment is also the crucial factor for controlling other film properties such as surface morphology,[16] density,[16,17] stress level,[18,19] crystallinity, grain size,[20,21] grain orientation, and chemical composition.

The crystal structures and surface morphology of IBAD ZrO_2 films produced at different deposition temperatures and their relationship to their hydrophilicity were investigated by transmission microscopy (TEM), atomic force microscopy (AFM), and contact angle measurements. TEM studies on these films revealed that these films are composed of nanocrystallites. The average nanocrystalline grain size of these films increases from 5 to 70 nm as the deposition temperature increases from room temperature to 550 °C. Tetrahedral structures on these ZrO_2 films can be observed by atomic force microscopy (AFM). These structures become very clear and distinct for samples produced at high temperatures (Figure SI.1, Supporting Information). Close

* Corresponding authors. E-mail: fnamavar@unmc.edu, ccheung@unlserve.unl.edu.

† Department of Orthopaedic Surgery and Rehabilitation, 985360 Nebraska Medical Center.

‡ Nebraska Centre for Materials and Nanoscience, University of Nebraska−Lincoln.

§ Department of Chemistry, University of Nebraska−Lincoln.

△ Department of Physics, University of Nebraska.

10.1021/nl072147v CCC: $40.75
Published on Web 03/14/2008

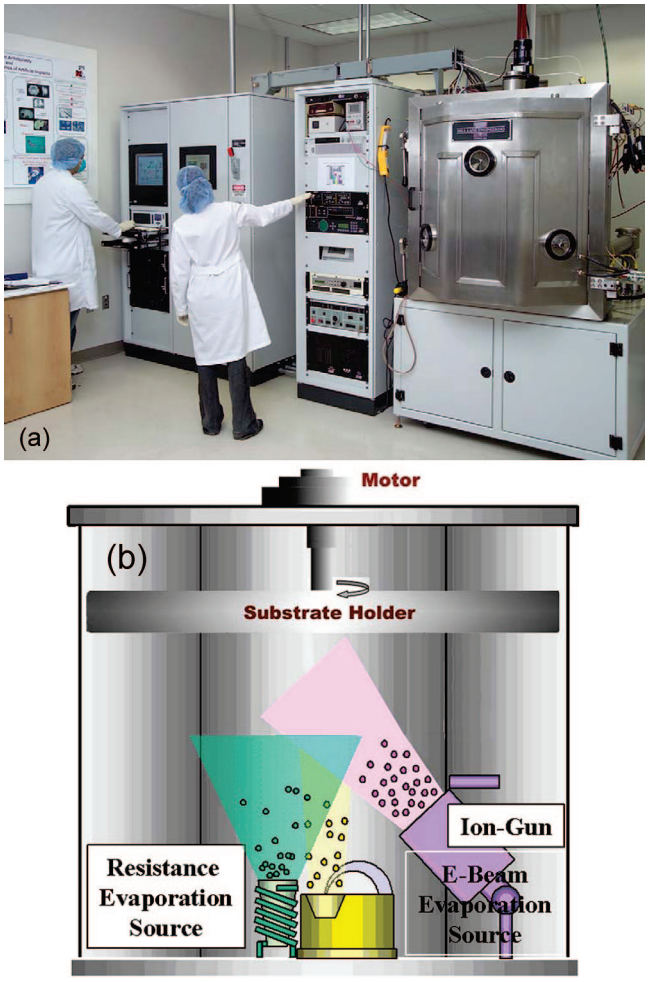

Figure 1. (a) IBAD system and (b) schematic. The process combines physical vapor deposition (evaporation) with concurrent ion beam bombardment to produce a wide range of nanocrystallites and coatings.

examination of these tetrahedral structures indicates that they possess 3-fold symmetry with axes symmetry perpendicular to the surface, along the direction the ion beam used during deposition. Both freshly prepared and aged (monitored up to 1 year) nanostructured ZrO_2 films were maximally wettable by water, demonstrating from zero to several degrees contact angles (CA) with an effective surface energy[22–24] (SE) of 82 dynes/cm as compared to CA of about 50° and SE of 59 dynes/cm for conventional chemically stabilized tetragonal phase of zirconia that are used for orthopedic implant devices.[25] In addition, our contact angle measurements on the smooth surface of commercially available single crystal of yttria (21%) stabilized cubic ZrO_2 also exhibits a contact angle of 50° for water. Higher wettability is obtained by having a higher effective surface energy, which is manifested by smaller contact angle. Wenzel[11] model proposes that by increasing the ratio of true surface area to apparent surface area ($A_{true}/A_{apparent}$), one can increase the wettability or increase the effective surface energy. In practice, the actual surface area can be modified to a desired surface morphology[26] or texture by directed (parallel) ion beam used in IBAD. By calculating the actual surface area of the tetrahedral nanostructures observed by AFM and determining their ratio to the apparent surface area, one can realize that this ultrahydrophilic behavior can be explained by the Wenzel model.[11]

Historically, the very low thermal conductivity (an order of magnitude lower than steel) and relatively high thermal expansion coefficient of zirconia makes it the ceramic material of choice[27] for virtually all critical thermal barrier coating applications. There are three phases[28] (Figure SI.2, Supporting Information) of zirconia: monoclinic, tetragonal (e.g., stabilized zirconia), and cubic (e.g., diamond simulant stabilized with about 20% impurities). Generally, pure zirconia in nature is in the monoclinic phase at room temperature. This phase is stable up to 1170 °C. Above this temperature, it transforms into the tetragonal phase, which then transforms into the cubic phase at above 2370 °C. During the cooling period, there is a characteristic 3−5% volume increase for the tetragonal to monoclinic phase change[29] and similar behavior occurs for the cubic to tetragonal phase change. During the cooling from high temperature, stresses generated because of this volume change cause cracks in pure zirconia ceramics that result in breakage of pure zirconia into pieces when cooled back to the ambient temperature.

One way to maintain stability of tetragonal and cubic phases at room temperature is to add trivalent stabilizing oxides such as Y_2O_3, CeO_2, MgO, and CaO to produce what is known as partially stabilized zirconia (PSZ). However, the mechanical properties of zirconia deteriorate with increasing concentrations of stabilizing oxides[30] above 8%. Formation of nanocrystalline cubic ZrO_2 with an average 15 nm grain size in powder form has been demonstrated by sol–gel, ball milling, and other techniques.[31–33] The tetragonal phase of zirconia has also been claimed for free nanocrystalline grains but with larger particle sizes.[33–37] However, it is problematic and impractical to produce adherent hard protective films utilizing ceramic powders.

The nanocrystalline ZrO_2 samples reported in this letter were prepared by ion beam assisted deposition at the Nanotechnology Laboratory of the University of Nebraska Medical Center (Figure 1). The IBAD system (Mill Lane Engineering, Lowell, MA) is composed of a Veeco 12 cm RF ion gun that supplies ions at energies up to 1500 eV with a total current density of 500 mA, which provides a broad uniform ion beam of oxygen, nitrogen, and argon, a DC ion gun with an ion density of 3 A at energies up to 150 eV, a thermal evaporation source, and a programmable sweep multipocket for electron beam evaporation source. IBAD experiments were carried out in an ultrahigh vacuum environment at a base pressure of 10^{-8} Torr. This is a unique approach to produce single and multilayer films with engineered surface properties that are not possible through conventional techniques. Using this ion beam technique, we can easily create a gradual transition (Figure SI.3, Supporting Information) between the substrate material and the deposited film with less built-in stress than other techniques. These properties result in films with a much more durable adhesion to the substrate even at room temperature. Ion bombardment also aids the production of stress-free films, eliminating

stress-induced problems such as buckling, microcracking, or peeling. It should be noted that although IBAD is applied to fabricate films with nanocrystal grains, these nanograins are not harmful[38] to the environment because they are tightly bound to each other and to the substrate and they are not free to move around in nature.

Source material for deposition was 99.7% pure ZrO_2 with a monoclinic crystal structure (lot number C01P41 Alfa Aesar, Ward Hill, MA). ZrO_2 deposited onto silicon, glass, quartz (for analytical testing), ultrahigh molecular weight polyethylene, and metallic substrates. Evaporation rate ranging from 1 to 4 Å/s, ion species (O, N, and Ar ions or mixtures), ion energy (0−600 eV), ion current density (0−500 μA/cm^2), and the substrate temperature ranging from room to 550 °C (aided by resistance heater) were optimized to produce ZrO_2 with specific nanograin structures. More than 100 depositions under different ion beam deposition conditions were carried out to produce nanostructured zirconia with ultrahigh wettability, hardness, and optical transparency. Rutherford backscattering spectroscopy (RBS) with 2.275 MeV He^{2+} beam and energy dispersive X-ray (EDX) were applied to analyze the chemical composition of zirconia films. EDX analysis, which was performed during TEM measurements, demonstrated the presence of only zirconium and oxygen.

The wetting behavior was observed by measuring the contact angle of a deionized (DI) water droplet on the surfaces of various nanocrystalline ZrO_2 samples using a computer-controlled video contact angle (VCA) instrument Optima XE from AST Product, Inc. A liquid droplet of 0.25 or 0.5 μL volume was dispensed from an automated syringe and brought into contact with the sample surface. The contact angle was then determined through video-image digitization and numerical curve-fitting using the Laplace equation of capillarity.[22–24] Ten drops were analyzed on each test component, with at least three test components for each deposition. Determination of surface energy[22–24] requires contact angle measurements on the surface, using two or more known fluids whose polar and dispersive components are known. We have calculated the effective surface energy of our coatings by the use of water and methylene iodide and application of SE-2500 software (AST Product, Inc.). This software can calculate surface energy based on either of three different known models[22–24] i.e., the harmonic,[39] geometric,[40] and acid–base models.[41] The surface morphology and crystal structure of the ZrO_2 films were characterized by atomic force microscopy (AFM), interferometry, X-ray diffractometry (XRD), and transmission electron microscopy (TEM).

Electron beam evaporation of elemental zirconium or powder zirconia with concurrent ion beam bombardment at room temperature resulted in formation of pure cubic phase ZrO_2. When elemental zirconium was used as a source material, a stoichiometric ZrO_2 was obtained (within accuracy of RBS) by a combination of oxygen bombardment and oxygen backfill. However, when powder zirconia (white color monoclinic ZrO_2 phase) was used as a source material for electron beam evaporation, a transparent stoichiometric

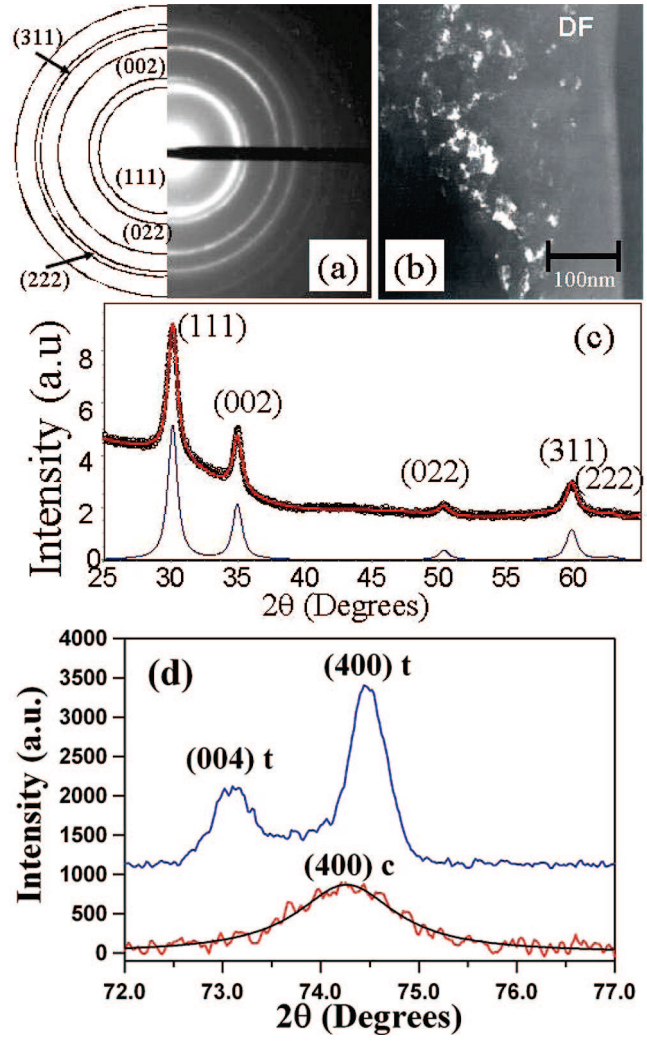

Figure 2. Proof of pure cubic zirconia, (a) electron diffraction and (b) dark-field TEM image demonstrating formation of nanocrystalline ZrO_2, with 5–8 nm size, at room temperature. Both (a) and (c) X-ray diffraction data are consistent with cubic phase formation. In particular, X-ray spectrum demonstrates an excellent fit for cubic phase with an average grain size of 12 nm ($\chi^2 = 1.43$). (d) Comparison of X-ray diffraction data from medical grade tetragonal zirconia (blue) and nanocrystalline ZrO_2 (red). The Lorentzian fitted cubic (400) peak (black) for the nanocrystalline ZrO_2 is estimated at 74.26 ± 0.01°. This single peak provides absolute proof for formation of cubic zirconia, see text for details.

ZrO_2 was obtained with all ions used, including oxygen and a mixture of oxygen with argon and nitrogen. This is not surprising because standard heat of formation (enthalpy) for ZrO_2 (−261.5 kcal/mol) is much smaller than that for ZrN, which is (−87.3 kcal/mol[42]). Zirconium metal is easily oxidized and stoichiometric zirconia forms if there is sufficient oxygen available. Furthermore, utilizing backfill of ultrapure oxygen ensures formation of stoichiometric ZrO_2. On the basis of our experiments, metal-rich ZrO_2 films appear gray or darkish, which is the result of inadequate availability of oxygen during deposition.

Figure 2 shows the dark-field TEM image of a typical ZrO_2 film deposited at room temperature using zirconia powder and an ion beam at 150 eV, which demonstrates equi-axed crystallites with dimensions of 5−8 nm. Grain size deter-

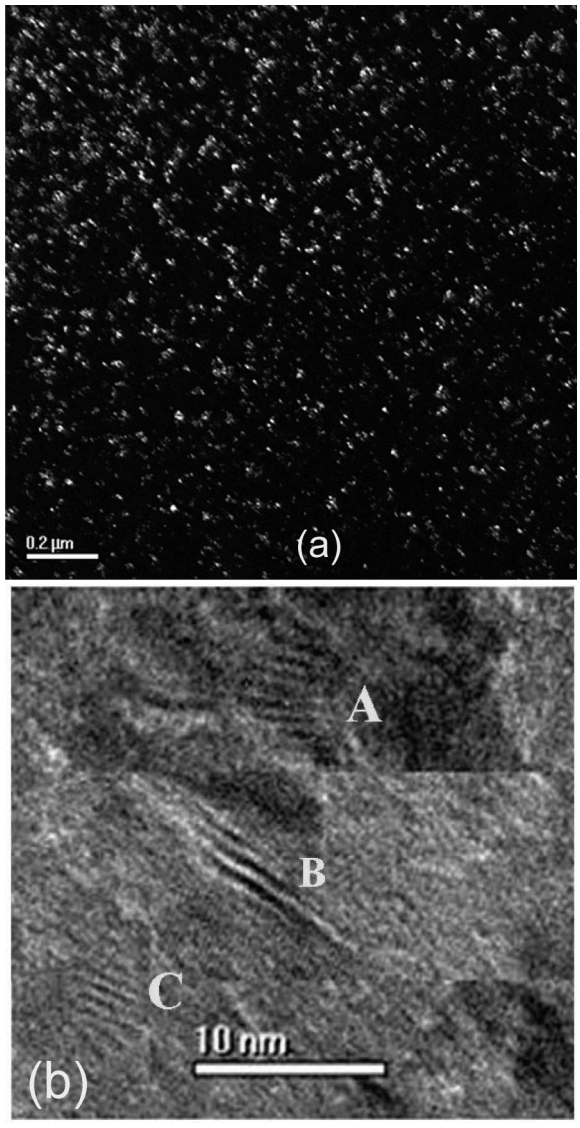

Figure 3. (a) Typical dark-field image for nanostructurally stabilized cubic zirconia with 5–8 nm size, (b) lattice fringes (actual nanocrystal labeled with A, B, and C) in a bright-field image of cubic zirconia.

mination was based on measuring the size of white/black spots in several dark/bright[43] field TEM images by a TEM specialist and then in our laboratory using several printed images such as Figure 3a. Figure 3b shows actual lattice fringes from nanocrystalline cubic ZrO_2 observed in a bright-field TEM image. Selected area electron diffraction (SAD)[43] of the film, when correctly exposed, shows the pattern as seen in Figure 2a. The observed pattern corresponds well to a cubic structure. However, the cubic and tetragonal patterns are very close and can be distinguished only from the splitting of the rings. The splitting is more evident in the high-order reflections. It can be stated that if the rings are split, a tetragonal phase is present. A careful examination of the high-order rings in a purposely overexposed SAD (not shown here) showed no splitting. Therefore, one can see that these results are consistent with that of the cubic phase of ZrO_2. Furthermore, the XRD spectra were compared to the ICDD PDF cards[44] representing powder patterns of three polymorphs of ZrO_2: monoclinic, tetragonal, and cubic. The peak positions for samples deposited at room temperature with a 150 eV ion beam match all the data for the cubic phase (PDF no. 49-1642).[44] Even the most intense reflections of the monoclinic phase, such as (111), are not apparent.

Although both SAD[43] (Figure 2a) and XRD (Figure 2c) results are consistent with the formation of cubic phase of ZrO_2, one may argue that these results do not provide an absolute proof of pure cubic phase formation. This is because the axial ratio, *c*/*a*, of the tetragonal phase[45,46] is in the range of 1.01 and 1.02 and X-ray diffraction (XRD) patterns associated with the cubic and tetragonal phases cannot easily be distinguished especially because of broadening of lines due to nanocrystalline structures. Recently, Lamas et al.,[45,46] in an elegant work, have shown that the (400) peak of cubic zirconia phase split into the (400) and (004) peaks, which is characteristic of the tetragonal phase. This separation is due to the elongation of cubic zirconia along one of the three equal axes of cubic fluorite type structures. It is interesting to realize that separation of (004) and (400) lines of the tetragonal phase zirconia is more than 1°.[46] Therefore, it can provide solid proof of the cubic or tetragonal phase even in nanocrystalline zirconia. The problem is that the (400) reflection is rather weak. Thus Lamas[45,46] applied synchrotron X-ray diffraction studies for differentiating the tetragonal phase from the cubic phase of nanocrystalline zirconia. However, we have applied conventional X-ray diffractometry using copper target generated X-rays with a Bruker general area detector diffraction system (GADDS), which allows high signal-to-noise XRD data collection. Figure 2d compares X-ray diffraction spectra for room temperature IBAD deposited nanocrystalline zirconia with a known chemically stabilized tetragonal phase of zirconia used for medical prostheses. The XRD spectrum of the tetragonal ZrO_2 clearly shows the splitting of the (400) line into (004) and (400) lines at 73.2° and 74.5° with intensities ratio of about 1:2. However, the XRD spectrum of the IBAD nanocrystalline sample shows only one (400) Bragg peak at 74.26°. This spectrum clearly demonstrates the symmetric shape of this Bragg peak from nanocrystalline zirconia and thus suggests that it is unlikely a merged peak from the (004) and (400) lines of the tetragonal phase due to the line broadening effect caused by the small crystallite size of the nanocrystalline. RBS spectra clearly demonstrated that cubic ZrO_2 films are indeed stoichiometric.[8]

The requirement for the nanocrystalline coating is that it should exceed the hardness of coated material because harder materials possess higher wear resistance. However, the most fundamental and essential property for any coating is adhesion.[12–15] Any surface coating without good adhesion is useless for practical application. Therefore, we apply routine scratch tests to examine the adhesion of all our IBAD coatings. We scratched the coatings with Mohs[47] hardness tester tools. Our minimum requirement for ZrO_2 coatings was that it should not scratch or separate by Mohs number 7 (quartz) hardness testers, which is equivalent to 12 GPa.[47] Furthermore, we have applied nanoindentation[48,49] techniques to measure hardness of our nanostructurally stabilized ZrO_2

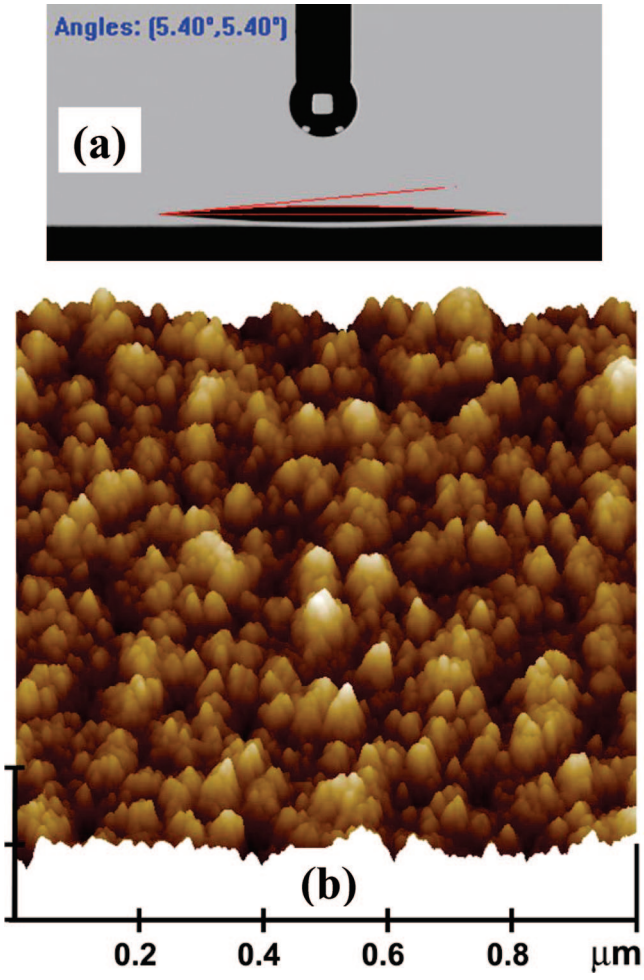

Figure 4. (a) Contact angle of cubic zirconia. Contact angle of a 0.25 μL water droplet on structurally stabilized nanocrystalline cubic ZrO_2 film produced at room temperature and measured a few days after deposition. A contact angle of 4 ± 0.5° measured after 10 months, keeping the sample in a laboratory environment. (b) AFM of the same sample, see larger and more clear nanostructures for deposition at higher temperature shown in Figure 6.

samples. As it was recently reported,[8] we have measured a nanohardness of about 16 GPa and a bulk modulus (239 ± 12 GPa) for nanostructurally stabilized cubic zirconia thin film. The measured bulk modulus is in good agreement with a model calculation based on projector augmented wave first-principles method (included in VASP package[9]) for chemically pure zirconia. We have found[8] that the bulk modulus of the cubic phase (237 GPa) is considerably larger than the bulk modulus of the monoclinic (155 GPa) and tetragonal phases (189 GPa). Recently it was reported that there was a nanohardness of 12.1 GPa[50] for oxidized[51] Zr-2.5Nb (monoclinic phase) and 15 GPa for stabilized tetragonal zirconia phase. Furthermore, first-principles calculations[9,10] indicated that that surface energy of the cubic phase is also larger than both the monoclinic and tetragonal phases.[10]

Figure 4 shows a typical contact angle result for a latter sample taken a few days after deposition at room temperature (January 15, 2004) that indicated a contact angle of about 5° for deionized water. Figure 4b demonstrates the AFM of this sample, where we measured a roughness of about 7 nm. Attempts have been made to monitor the effect of aging of the wettability of these samples. Latter samples kept in a laboratory environment for approximately 10 months and then remeasured (on October 13, 2004), without any cleaning, obtained a contact angle of 4 ± 0.5°. For several other nanostructurally stabilized cubic pure ZrO_2 samples, the relationship of contact angles and aging were also monitored for about a year. As this manuscript was in the process of preparation, we have again reexamined samples from 10 IBAD runs that were produced during the past 3 years; again, our experiments confirmed the earlier results, i.e., total water wettability. Furthermore, samples annealed at 400 °C were measured for their contact angles where we have attained a contact angle of about 10° (see Table 1). The contact angle stability is consistent with our recent results that have demonstrated[8] chemical stability up to 1000 °C and cubic phase stability up to 850 °C for these samples.

In summary, IBAD nanocrystalline ZrO_2 films that were produced at room temperature by a directed (parallel) ion beam exhibited significant water wettability with strong dependence on the deposition conditions. Typical nanostructurally stabilized ZrO_2 wettability measured angles are in the range of 0−10° in contrast to a set of ZrO_2:

(I) Samples produced by sputtering technique have measured (under identical conditions) contact angles of about 50−70°.

(II) Well polished and smooth chemically stabilized tetragonal zirconia phase (with microsize crystals and a nanohardness of 15 GPa,[50] which are used as artificial orthopedics implants) were studied to determine their contact angles. An average contact angle of about 50° has been measured[25] for statistically significant numbers of these implant devices.

(III) The monoclinic phase of zirconia (oxidized Zr-2.5Nb52 alloy[51] with microsize crystals and a nanohardness of 12 GPa[50]) is a stable phase at room temperature, where again we have also measured[25] contact angles of 50° or more.

(IV) Commercially available chemically stabilized (21%) transparent single crystal cubic zirconia exhibited a contact angle of about 50°. We have measured a nanohardness of few GPa for these materials. This is not surprising because it is well-known that mechanical properties of zirconia are dependent[30] on the concentration of stabilizing oxides and mechanical properties deteriorate when concentration stabilizing oxide is above 8%.[30]

Figure 5 shows two images of advancing contact angles selected out of 100 recorded frames (10 frames/s) for a ZrO_2 film deposited at 375 °C. A zero contact angle can be observed after 2.08 s of droplet deposition. To explain the origin of wettability of our zirconia films, the surface morphology of ZrO_2 samples was studied by AFM where the presence of pyramidal nanostructures was observed. These pyramidal surface structures are pronounced and undisputable for samples deposited at temperatures at or above 300 °C. A typical example of these structures deposited at 375 °C is shown in Figure 6a. In Figure 6a and other AFM images, triangular hillocks and occasional larger triangular terraces are eminent. The diameters of the hillocks or tetrahedral nanostructures in Figure 4a are in the range

Table 1. Components of Contact Angle for 0.5 μL Water Droplet Measured for a Nanostructurally Stabilized Cubic ZrO_2 Annealed in Air at 400 °C

index (unit)	left angle, deg	right angle, deg	width, mm	height, mm	area, mm^2	volume, μL
mean	10.6 ± 1.8	10.6 ± 1.8	3.0 ± 0.2	0.14 ± 0.02	7.3 ± 1.1	0.52 ± 0.15

of 130–210 nm. The mean roughness (R_a) is about 17 nm, which is in good agreement with those obtained by an interferometer for an area of 500 by 500 μm^2. In addition, it appears that these tetrahedral structures possess 3-fold symmetry but in plane rotational disorder. This symmetry axis is typically along the direction of the ion beam used during deposition. These tetrahedral structures were also observable in TEM images; however, they became clearer at higher deposition temperatures. Again, on the basis of several dark-field images, the grain size of ZrO_2 film deposited at 375 °C range from 10 to 60 nm (a typical example is shown in Figure 6c); as compared to the samples deposited at room temperature, the latter samples have a much larger grain size (about >5–10 times larger).

The finite AFM tip size (about 10 nm in diameter) leads to the dilation of imaged features and thus underestimation of the actual surface area for samples deposited at room temperature with nanocrystallites of about 5–8 nm. Therefore, results with larger grains such as those shown in Figure 6a are important for the estimation of actual surface area with higher accuracy because the AFM tip convolution effect is much reduced with imaged features much larger than the AFM tip size. Thus, the calculated actual surface areas and Wenzel ratios from these AFM data would be less underestimated and closer to the actual values.

X-ray diffraction measurements of samples deposited at higher temperature indicated the formation of cubic structures with some monoclinic and structures. These samples, kept in ambient laboratory conditions and monitored by contact angle measurements up to about 100 days after coating, also exhibited contact angles of less than 5°.

We applied the Wenzel model[11] to explain the ultrahydrophilic properties of the zirconia films. The contact angle φ measured on a rough or nanostructurally designed textured surface is related to the equilibrium Young angle θ (for an ideally smooth surface) through the Wenzel relation: $\cos \varphi = r \cos \theta$ *or* $\cos(\theta_{\text{apparent}}) = r \cos(\theta_{\text{Young}})$. The r is the ratio of the true wetted area to the apparent area (Figure 7). Wenzel's result was derived for idealized rough surfaces by

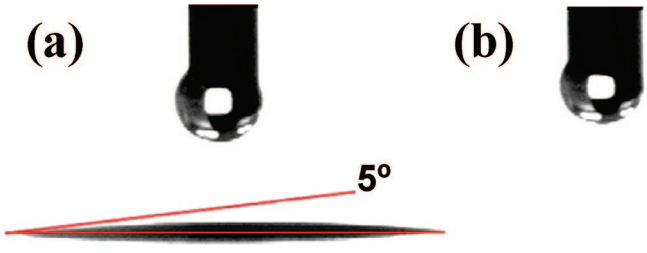

Figure 5. Video camera image of contact angle of zirconia showing the spreading of a 0.25 μL water droplet on a nanocrystalline ZrO_2 film produced at 375 °C. After the droplet was brought in contact with the surface, the total time for the droplet to spread was 2.08 s. Afterward, the contact angles measured for time frames (a) t = 1.75 s and (b) 2.08 s are 5° and 0°, respectively.

Johnson and Dettre[52] and Dettre and Johnson.[53] The essence of the theory is that apparent contact angle on the rough surface is connected with the contact angle of a smooth surface (Young's angle). It means that at some critical Young's angle, the cosine of the apparent angle will be 1, i.e., the apparent contact angle is zero. It is a condition of complete wetting or wicking. Wenzel's ratio indicates strong modification of the apparent contact angle compared with the one on the smooth surface such as surface single crystal ZrO_2. When the Young's angle θ is less than 90°, based on the Wenzel relation, the contact angle on the nanostructurally designed surface should be smaller than the contact angle on the smooth surface. On the other hand, when the Young's angle θ is greater than 90°, again based on the Wenzel relation, a rough surface became hydrophobic, similar to lotus leaves. In other words, Wenzel's ratio acts as a factor to amplify the hydrophobic or hydrophilic properties. To our knowledge, the contact angle of pure cubic or pure tetragonal zirconia have not been measured mainly because cubic and tetragonal zirconia have been produced in loose nanoparticles.

We have performed measurements of contact angle on the smooth surface of single crystal commercially produced yttria stabilized cubic ZrO_2 and well-polished smooth chemically stabilized tetragonal zirconia of orthopedics implants that exhibited[25] contact angles of about 50° and 55°, respectively. On the basis of these measurements and absence of these materials in pure form, we assume that the contact angle for pure and smooth surfaces should be the same as those measured for chemically stabilized phases (i.e., about 50°). Therefore, we use 50° as a reference contact angle, i.e., Young's angle θ for Wenzel relation. From above Wenzel equation, the critical Wenzel's ratio at which complete wetting occurs is 1.55 ($r = \cos(50°)^{-1}$ where $r \cos 50° = \cos 0 = 1$). Using large number AFM images, we have estimated actual surface area that Wenzel's ratio is in range of 1.5−2.7. Obviously ultrahydrophilic properties of these surfaces indicate that the Cassie−Baxter[54] model (frequently employed for hydrophobic rough surfaces) is not applicable to these particular nanostructured materials. The complete wetting conditions obtained by Wenzel's equation (which describes equilibrium contact angle) are supported by free energy analysis of the droplet on the surfaces, mimicking experimental results.

In summary, we have produced by IBAD process, dense, hard,[8] and adherent nanocrystalline zirconia. SAD[43] and X-ray diffraction results clearly show the presence of only cubic phase zirconium oxide for samples deposited at room temperatures. Ion beam bombardment is essential to produce pure cubic phase as physical vapor deposition alone resulted in the formation of mixed phases. For deposition at a higher temperature (e.g., 400 °C), the presence of monoclinic phase appeared in conjunction with cubic phase. The absence of a

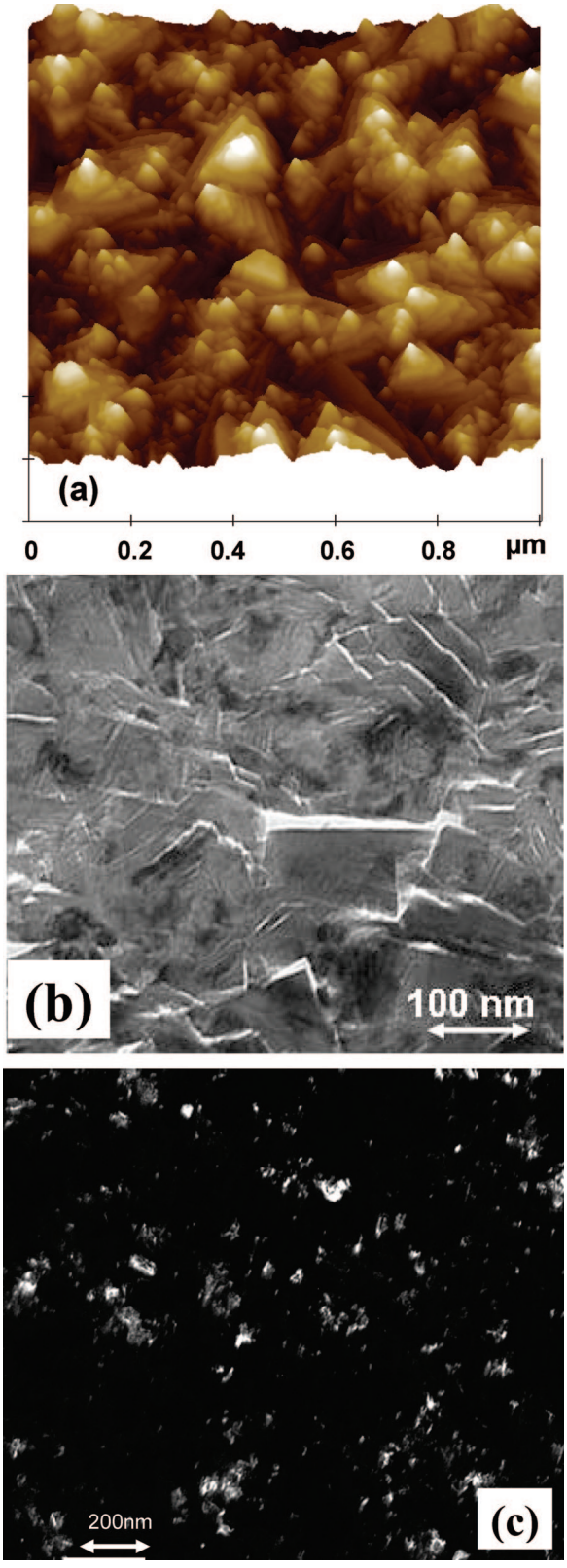

Figure 6. Images of zirconia showing pyramidal nanostructures. (a) AFM Image of the ZrO_2 film shows tetrahedral structures with 3-fold symmetry but in plane rotational disorder, deposited onto a silicon substrate. The z-scale is 200 nm/div. The measured mean roughness (R_a) of 1 μm^2 is about 17 nm. (b) A typical bright-field TEM image also showing tetrahedral structures. (c) A typical dark-field TEM image of ZrO_2 deposited at 375 °C, showing 30–60 nm nanocrystallites. See text for details.

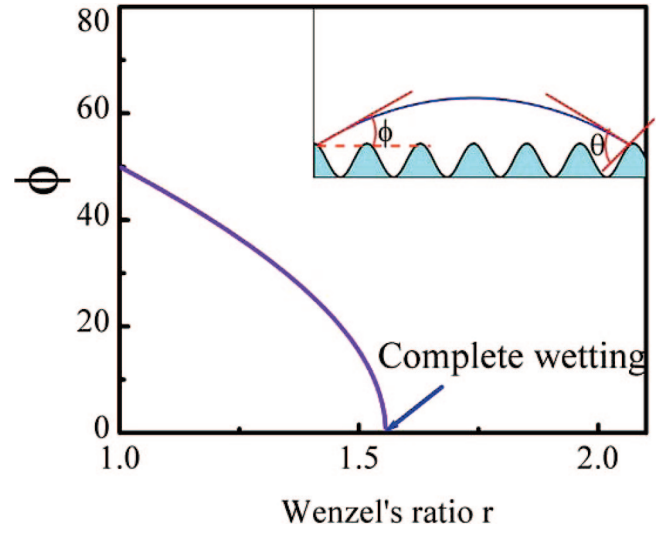

Figure 7. Theoretical modeling of contact angle for zirconia. Theoretical calculation of water contact angles, Calculation of angles on nanostructured ZrO_2 film as a function of the Wenzel's ratio (r). Inset: theoretical apparent contact angle model. Angle φ is apparent contact angle and θ is Young's contact angle of the smooth surface.

chemical stabilizing agent and the absence of porosity, which is a consequence of ion beam bombardment, resulted in hardness of the cubic phase of zirconia. As we have shown[8] recently, the hardness of nanostructurally stabilized cubic ZrO_2 is about 16 GPa versus few GPa for commercially cubic zirconia with 21% chemical stabilizer. This is because the mechanical properties of zirconia deteriorate with increasing concentrations of stabilizing oxides[30] above 8%. It should be noted once more that conventional cubic and tetragonal zirconia with micrograin are not stable at room temperature and require up to 20% chemical stabilizer to prevent breakage due to phase transformation during cooling period.

We have also demonstrated fabrication of ultrahydrophilic pure nanocrystalline cubic zirconium oxide films that possess a complete wetting to water. Excellent wetting properties and larger effective surface energy of these samples are partially due to a large apparent tetrahedral surface area, which yields a hydrophilic surface with complete wetting. It is apparent that directed (parallel) ion beam bombardment is essential to produce hydrophilic surface as compared to samples produced by the sputtering technique (with multi-directional ion bombardment), which rendered contact angles of about 50° or higher. The ultrahydrophilic property was explained by the Wenzel model,[11] i.e., large ratio (1.5−2.7) of actual surface area to apparent surface area. In contrast to titanium oxides[3] that show zero contact angles for a short time, our aged nanocrystalline zirconia films maintained high wettability over increased length of time. The combination of hardness and wettability of ZrO_2 film will have important implications for asymmetric (hydrophilic−hydrophobic) articulating surfaces such as a *Janus Interface*[55] with a hydrophilic surface on one side to contain the lubricant and a hydrophobic surface on the other side to force it (lubricant) away. While the hydrophilic surface maintains the lubricant, the hydrophobic surface creates a low-viscosity boundary

between the hydrophobic surface and lubricant,[55] therefore producing a low friction condition.

Because of the possibility of room temperature deposition of ultrahydrophilic cubic ZrO_2, all material including polymer can be coated with excellent adhesion and without degradation to the substrates. Therefore, it may also have implications for biomedical application where an ultrahydrophilic surface is required such as DNA microarray,[56] tissue engineering,[57] and cell adhesion and proliferation.[58,59]

Acknowledgment. We thank the Nebraska Research Initiative, the University of Nebraska Medical Center, the University of Nebraska at Omaha, and the University of Nebraska−Lincoln for their support. We are grateful to Professor Michael Graham (Northwestern University) for the nanohardness measurements, Dr. H. Kawayoshi (AMER, Inc.) and Dr. R. Ayer (STEM, Inc.) for the TEM measurements.

Supporting Information Available: AFM image ZrO_2 deposited at 375°C; phase transition and crystal structures of zirconia; an ideal coating: functionally graded nanocrystalline coating with a gradual reduction of grain size and modification of chemistry from substrate to surface provides strong bonding between coating and substrate. This material is available free of charge via the Internet at http://pubs.acs.org.

References

(1) Lafuma, A.; Quere, D. *Nat. Mater.* **2003**, *2*, 457.
(2) Blossey, R. *Nat. Mater.* **2003**, *2*, 301.
(3) Wang, R.; Hashimoto, K.; Fujishima, A.; Chikuni, M.; Kojima, E.; Kitamura, A. *Nature* **1997**, *388*, 431–432.
(4) Hirvonen, J. K. *Mater. Res. Soc. Symp. Proc.* **2004**, 792, R12.5.1.
(5) Nastasi, M.; Mayer, J. W.; Hirvonen, J. K. *Ion−Solid Interactions: Fundamentals and Applications*; Cambridge University Press: New York, 2004.
(6) Mattox, D. M. *Handbook of Physical Vapor Deposition (PVD) Processing*; Noyes Publications: Park Ridge, NJ, 1998.
(7) Hirvonen, J. K. *Mater. Sci. Rep.* **1991**, *6*, 215.
(8) Namavar, F.; Wang, G.; Cheung, C. L.; Sabirianov, R. F.; Zeng, X. C.; Mei, W. N.; Bai, J.; Brewer, J. R.; Haider, H.; Garvin, K. L. *Nanotechnology* **2007**, *18*, 415702.
(9) Kresse, G.; Furthmuller, J. *Phys. Rev. B* **1996**, *54*, 11169.
(10) Christensen, A.; Carter, E. *Phys. Rev. B* **1998**, *58*, 8050.
(11) Wenzel, R. N. *Ind. Eng. Chem.* **1936**, *28*, 988.
(12) Baglin, J. E. E. Interface Structure and Thin Film Adhesion. In *Handbook of Ion Beam Processing Technology*, eds. Cuomo, J. J., Rossnagel, S. M., Kaufman, H. R., Eds.; Noyes Publications: Park Ridge, NJ, 1989; Chapter 14.
(13) Mattox, D. M.; Cuthrell, R. E. Residual Stress Fracture and Adhesion in Sputter-Deposited Molybdenum Films. In *Adhesion in Solids*; Mattox, D. M., Baglin, J. E. E., Gottschall, R. E., Batich, C. D., Eds.; MRS Symposium Proceedings, *Vol. 119*; Materials Research Society: Warrendale, PA, 1988; p 141.
(14) Kellock, A. J.; Baglin, J. E. E.; Barlin, T. T. *Phys. Res. B* **1991**, *59/60*, 249.
(15) Namavar, F.; Colter, P.; Karimy, H.; Tobin, E.; Jollimore, C.; Yoganathan, M. Nanocrystalline, Superhard, Ductile Ceramic Coatings for Roller-Cone Bit Bearings. In *Proceedings Geothermal Program Review XV, The Role of Research in the Changing World of Energy Supply, San Francisco, California, March 24-26, 1997*; DOE/EE-0139, U.S. Department of Energy, Office of Geothermal Technologies, 1997, 5-47–5-58, http://192.107.175.222/geothermal/product.biblio.jsp?osti_id=603434&query_id=0&page=0. Spire Researchers Making Progress. In *Geothermal Technologies Quarterly Bulletin*; U.S. Department of Energy; 1999; *Vol. 4* (1), p5, http://www1.eere.energy.gov/geothermal/pdfs/grc2-99.pdf.
(16) Müller, K. H. *Phys. Rev. B* **1987**, *35*, 7906.
(17) Müller, K. H. *J. Appl. Phys.* **1986**, *59*, 2803.
(18) Müller, K. H. *J. Appl. Phys.* **1987**, *62*, 1796.
(19) Cuthrell, R. E.; Mattox, D. M.; Peeples, C. R.; Dreiike, P. L.; Lamppa, K. P. *J. Vac. Sci. Technol., A* **1988**, *6*, 2914.
(20) Roy, R. A.; Cuomo, J. J.; Yee, D. S. *J. Vac. Sci. Technol., A* **1988**, *6*, 1621.
(21) Namavar, F.; Haupt, J.; Tobin, E.; Karimy, H.; Trogolo, J.; Colter, P.; Yoganathan, M.; Jollimore, C.; Bricault, R.; Hirvonen, J. P.; Ayer, R. *Mater. Res. Soc. Symp. Proc.* **1997**, *438*, 709–714.
(22) Good, R. J. *Modern Approaches to Wettability: Theory and Applications*; Schrader, M. E., Loeb, G. I., Eds.; Plenum Press: New York, 1992; pp 1–27.
(23) Wu, S. *Polymer Interface and Adhesion*; Marcel Dekker: New York, 1982.
(24) Mittal, K. L. *Contact Angle: Wettability and Adhesion*; VSP BV: Utrecht, The Netherlands, 1993.
(25) Salehi, A. T.; Tsai, S.; Pawar, V.; Sprague, J.; Hunter, G.; Varma, S.; Namavar, F. *Key Eng. Mater.* **2006**, 309–311.
(26) Wang, G.; Brewer, J. R.; Namavar, F.; Sabirianov, R. F.; Haider, H.; Garvin, K. L.; Cheung, C. L. *Scanning*, **2008**, *30*, 59–64.
(27) Samsonov, G. V. *The Oxide Handbook*, 2nd ed.; FI/Plenum: New York, 1982; p 120.
(28) Winkler, M. F.; Parker, D. W. *Adv. Mater. Process.* **1992**, *141*, 17–22.
(29) Kvernes, I. In *High Tech Ceramics*; Elsevier Science: Amsterdam, 1987; pp 2519–2536.
(30) Lange, F. F. *J. Mater. Sci.* **1982**, *17*, 225–234.
(31) Bouvier, P.; Djurado, E.; Lucazeau, G.; Hihan, T. L. *Phys. Rev. B* **2000**, *62*, 8731–8737.
(32) Gateshki, M.; Petkov, V.; Williams, G.; Pradhan, S. K. R. *Phys. Rev. B* **2005**, *71*, 224107.
(33) Lajavardi, M.; Kenney, D. J.; Lin, S. H. *J. Chin. Chem. Soc.* **2000**, *47*, 1043–1053.
(34) Rush, G. E.; Chadwick, A. V.; Kosacki, I.; Anderson, H. U. *J. Phys. Chem. B* **2000**, *104*, 9597–606.
(35) Shukla, S.; Seal, S. *Int. Mater. Rev.* **2005**, *50*, 45–64.
(36) Shukla, S.; Seal, S.; Vij, R.; Bandyopadhyay, S. *Nano Lett.* **2003**, *3*, 397–401.
(37) Shukla, S.; Vij, R.; Bandyopadhyay, S.; Rahman, Z. *Nano Lett.* **2002**, *2*, 989–993.
(38) Oberdörster, G.; Oberdörster, E.; Oberdörster, J. *Environ. Health Perspect.* **2005**, *113*, 823−839.
(39) Wu, S. *J. Polym. Sci., Part C* **1971**, *34*, 19.
(40) Owens, D. K.; Wendt, R. C. *J. Appl. Polym. Sci.* **1969**, *13*, 1741.
(41) Van Oss, C. J.; Good, R. J.; Chaudhury, M. K. *Langmuir* **1988**, *4*, 884.
(42) Karapetyants, M. K.; Karapetyants, M. L. *Thermodynamic Constants of Inorganic and Organic Compounds*; Ann Arbor Humphrey Science: London, 1970.
(43) Williams, B.; Carter, C. B. *Transmission Electron Microscopy: A Textbook for Materials Science*; Williams, D. B., Carter, C. B., Eds.; Springer: New York, 1996.
(44) Powder Diffraction File. PDF-2. International Centre for Diffraction Data: Newtown Square, PA, 2001; pp 19073–3273.
(45) Lamas, D. G.; Fuentes, R. O.; Fabregas, I. O.; Fernandez de Rapp, M. E.; Lascalea, G. E.; Casanova, J. R.; Walsoe de Reca, N. E.; Craievich, A. F. *J. Appl. Crystallogr.* **2005**, *38*, 867.
(46) Lamas, D. G.; Rosso, A. M.; Suarez, M.; Anzorena, A. F.; Fernandex, A.; Bellino, M. G.; Cabezas, M. D.; Walsoe de Reca, N. E.; Craievich, A. F. *Scr. Mater.* **2006**, *55*, 553.
(47) Whitney, D. L.; Broz, M.; Cook, R. F. *Am. Mineral.* **2007**, *92* (2–3), 281–288.
(48) Oliver, W. C.; Pharr, G. M. *J. Mater. Res.* **1992**, *7*, 1564.
(49) Doerner, M. F.; Nix, W. D. *J. Mater. Res.* **1986**, *1*, 601.
(50) Long, M.; Riester, L.; Hunter, G. Nanohardness measurements of oxidized Zr-2.5Nb and various orthopaedic materials. In *Transactions of the 24th Annual Meeting of the Society for Biomaterials, San Diego, California, April 22−26, 1998*; Society for Biomaterials: Minneapolis, MN, 1998; p 528.
(51) Hunter, G.; Dickinson; J.; Herb, B.; Graham, R. Creation of Oxidized Zirconium Orthopaedic Implants. *J. ASTM Int.* **2005**, *2* (7); http://dx.doi.org/10.1520/JAI12775.
(52) Johnson, R. E.; Dettre, R. H. Contact angle hysteresis, I. Study of an idealized rough surface. In *Contact Angle in Wettability and Adhesion*; Gould, R. F., Ed.; *ACS Advances in Chemistry Series 43*; American Chemical Society: Washington, DC, 1964; pp 112–135.
(53) Dettre, R. H.; Johnson, R. E. Contact angle hysteresis, II. Contact angle measurements on rough surfaces. In *Contact Angle in Wettability*

and Adhesion; Gould, R. F., Ed.; *Advances in Chemistry Series 43*; American Chemical Society: Washington, DC, 1964; pp 136–144.
(54) Cassie, A. B. D.; Baxter, S. *Proc. Faraday Soc.* **1944**, *40*, 546–551.
(55) Zhang, X.; Zhu, Y.; Granick, S. *Science* **2002**, *295*, 663.
(56) Blossey, R.; Bosio, A. *Langmuir* **2002**, *18*, 2952–2954.
(57) Hallab, J. N.; Bundy, K. J.; O'Conner, K.; Moses, R. L.; Jacobs, J. J. *Tissue Eng.* **2001**, *7*, 55–71.
(58) Namavar, F.; Jackson, J. D.; Sharp, J. G.; Mann, E. E.; Bayles, K.; Cheung, C. L.; Feschuk, C.; Varma, S.; Haider, H.; Garvin, K. L. *Mater. Res. Soc. Symp. Proc.* **2007**, *954*, 0954-H04-04.
(59) Jackson, J. D.; Sharp, J. G.; Haider, H.; Garvin, K. L.; Namavar, F. Preliminary analysis of attachment, survival and growth of bone marrow stromal cells on nanocrystalline hard ceramic coatings. *Ceramics, Cells and Tissues, 10th Seminar and Meeting on Materials for Scaffolding of Biologically Engineered Systems Interfaces and Interactions on a Nanoscale, Faenza Italy, May 2006*; Ravaglioli, A., Krajewski, A., Eds.; Consiglio Nazionale Delle Ricerche: Rome, 2006; p 109.

NL072147V